Beating heart implantation of transventricular artificial cordae: How can access site selection and leaflet insertion improve mitral regurgitation correction?

Luigi Di Micco[a], Benedetta Biffi[b], Silvia Schievano[b], Daniela P.Boso[a], Laura Besola[c,d], Alessandro Fiocco[d], Gino Gerosa[d], Francesca M. Susin[a], Andrea Colli[d,e], Paolo Peruzzo[a]

[a] Cardiovascular Fluid Dynamics Laboratory, ICEA Department, University of Padova, Via Loredan 20, Padova, 35131, Italy

[b] University College London, Institute of Cardiovascular Science & Great Ormond Street Hospital for Children, London, United Kingdom

[c] University of British Columbia, St Paul's Hospital Department of cardiovascolar surgery, Vancouver, Canada

[d] DSCTV, University of Padova Medical School, Italy

[e] Department of Surgical, Medical and Molecular Pathology and Critical Care Medicine, University of Pisa, Pisa, Italy

Abstract

NeoChord-DS1000-System (NC) and The Harpoon-Mitral-Repair-System (H-MRS) are two trans-apical chordal implantation devices developed for the treatment of degenerative mitral valve (MV) regurgitation (DMR) either if as Fibroelastic-Deficiency (FED), Forma-Frusta (FF), or Barlow (B) presentation. The aim of this study is to evaluate some of the advantages and disadvantages of these two different devices by performing numerical simulation analyses focused on different transventricular access sites in all subsets of DMR presentations. By applying a novel approach for the development of patient-specific MV domains we worked out a set of numerical simulations of the artificial chordae implantation. Different leaflet insertions and ventricle access sites were investigated, and resulting contact-area (CA), tensioning-forces (F) and leaflet's stress (LS) were calculated. The analyses showed that: i) NC-approach maintains low LS when performed with a posterior access site and optimizes the overlap between the leaflets at the systolic peak; ii) H-MRS-system presents better results in case of a more anterior ventricular entry site; however, for FED prolapse large variation of F and LS with respect to NC-approach are found; iii) an accidental contact between artificial sutures and the anterior leaflet may occur when valve function is restored through an excessive anterior access site. Present findings set light on specific technical aspects of transapical off-pump chords implantation, either performed with NC and H-MRS systems and highlight the advantages and disadvantages proper to the two devices. Our study also paves the basis for a systematic application of computational methodology, in order to plan a patient-specific mini-invasive approach thus maximizing the outcomes.

Keywords

Mitral valve, Mitral valve repair, Neochord, Harpoon, Miitral regurgitation, ePTFE, Transapical

1. Introduction

The transapical off-pump MV repair with artificial chords implantation has emerged as a new minimally-invasive therapeutic option to restore MV regurgitation due to prolapse or flail [1], [2], [3], [4], [5], [6], [7], [8], [9]. Currently, the procedure is mainly performed using the Neochord-DS1000-system (NC, St.Louis Park, MN), which delivers the artificial sutures on the free margin of the diseased leaflet through a postero-lateral left ventricle (LV) access site [10]. More recently an alternative device, the Harpoon-Mitral-Repair-System (H-MRS; Edwards Lifesciences, Irvine, CA), has been proposed to treat MV regurgitation. H-MRS is designed to implantat the artificial chordae directly into the leaflet body, beyond the rough zone, using a more anterior LV access site [11, 12].

In the last two decades, numerical simulations were largely used to assess the effectiveness of cardiovascular devices and surgical procedures [13], [14], [15], [16]. In particular the use of simulations of prolapsed heart valves is costantly increasing since it provides the numerical quantification of the effectiveness of a potential repair easing decision-making. [17]. Different research groups performed finite element analysis (FEA) of MV dynamics and the efficacy of MV repair surgical procedures [16, 18, 19, 20]. Other groups analysed the effects of different repair techniques (artificial neochords implantation, leaflet resection [21], edge-to-edge repair [21], [22], [23], [24], annuloplasty [25, 26]) on posterior leaflet disease MV models. Recently, a simplified comparative study concerning the optimization of the tensioning protocol for the NeoChord technique was published [27].

The aim of the present study is to investigate, using numerical simulations, the treatment of the three subsets of degenerative MV disease considering two different devices and different transventricular access sites. For this purpose, in-silico repair of the following 3 patient-specific MV diseases was simulated. The first case is an isolated FED. The peculiarity of this degenerative MV is the collagen deficiency that leads to thin transparent leaflets and, typically, to the rupture of thin chords. In long-term prolapse, secondary myxomatous pathologic changes may occur in the prolapsing segment, resulting in thickening and expansion of the leaflet. The second case is a Forme fruste (FF) MR. FF designates degenerative disease with excess tissue with myxomatous changes in usually more than one leaflet segment. In the third case, which is focused on a Barlow's disease (B), the hallmarks are large valve size, with diffuse myxomatous changes, and excess leaflet tissue, with thickened, elongated, and often ruptured chordae.

The aim of the present work is to show how different devices (NeoChord and Harpoon) and different ventricle access sites, which typically range in the treatment of Mitral valve prolapse from posterior (0°) to anterior (50°) position, significantly impact the leaflet coaptation, chords tensioning, and leaflet stress. This analysis was focused on three different prolapse typologies,

namely, FED, Forme Fruste, and Barlow. The results of our investigation provide an overview of the pros and cons of different implants techniques to surgeons.

2. Methods

We analysed and quantified the impact on MV function of LV access site and device type for transapical articial neochordae implantation. Three different MV prolapse subsets, Barlow disease (B), Forma Frusta (FF) and Fibroelastic deficiency (FED), [28] were considered and tensioning forces (F), leaflet's stress (LS) and coresponding contact area (CA) were computed for each case.

2.1. Design of the MV models

The MV model was designed through the careful segmentation of imaging data. The detailed shape of MV annulus and leaflets was obtained from three-dimensional echocardiography (3D-echo) and Computed Tomography (CT) datasets.

Preoperative 3D-echo datasets of all patients treated with transapical chordal implantation at the Cardiac Surgery Unit-University of Padua were analysed and patients were classified according to the specific MV disease subset (FED, FF, B). On this cohort we applied an ad-hoc post-procesing imaging model to derive three different patient-specific models, one for each MV disease subset.

In order to avoid any possible segmentation-related inaccurancy due to inadequate data, we selected the three cases with the best image definition and dataset quality.

Our selection methodology complies with the work by Hjortnaes J. and co-workers [29], who described the main differential pathomorphological features of B and FED with high accuracy, giving quantitative indications about leaflets redundancy, thickness, and annular dimension, etc. (see Table 1). In our case, three-dimensional transesopageal echocardiographic (3D echo) images of the MV were segmented by means of an automatic atlas-based segmentation-method, able to annotate MV leaflets and annulus [30]. The obtained segmentations were converted into smooth triangular mesh representations, thus providing patient specific leaflet geometry information at end-diastolic configuration (see Fig. 1). All main geometrical parameters of valve models are summarized in Table 1 for each prolapse type (B, FF, end FED). In detail, the segmentation analysis had permits to extract with high accuracy the following dimensional quantities used for our MV models: (LLd) intecommissural-distance, (APd), anteroposterior-diameter, (AMLl) anterior and (PMLl) posterior mitral leaflet lengths, (Ls) Leaflets surface, (MAp) Annulus perimeter, end (As) Annulus surface, thickness (t), Anterior leaflet (AL), Posterior leaflet (PL). The average anterior and posterior leaflet thickness was computed from the segmentation and used in the patient-specific numerical

model definition. The relative small variability allowed us to assume a constant thickness for the two leaflets, thus simplifying the model setup [22, 25, 31].

Computed tomography (CT) images were also analysed to gather information about the position of the papillary muscles (PMs) throughout the cardiac cycle. Specifically, a marker was manually placed on the PMs tip at each of the 10 CT frames, and its coordinates were exported. Finally, the interpolation was performed by using a piecewise cubic-spline. PMs displacements provide the dynamic boundary conditions for the numerical analysis throughout the cardiac cycle.

As widely recognised, the annulus reaches its maximum size in diastole, while at the end of the systolic phase it shrinks to its minimum dimension. The analysis of the CT-images, showed a reduced annulus movement and a consequent negligible reduction of the MV area at the end-systolic phase. Therefore we decided to maintain a constant MV Annulus dimension during the simulation of the closing phase.

Neither 3D echo nor CT images allowed the visualization of the chords structures, therefore they were assumed a posteriori by tuning the trajectories of the chords in ad hoc preliminary analyses. First, a set of native chordae was defined according to the PMs position and the leaflets free margin profile. A simulation of MV closing was then performed and, by a trial-and-error procedure, the number, the length, and the distribution of such native chordae were adjusted until a proper coaptation of the leaflets was recorded. The prolapse position and width were finally reproduced by a further trial-and-error procedure in which a limited number of virtual chords were detached (i.e., eliminated) or elongated as long as a good agreement between the simulated and the reconstructed prolapse was found.

Therefore, MV function was restored by inserting artificial chords in the virtual model. In agreement with the surgical clinical practice, three chords were added for the B prolapse and four chords for the FED and the FF prolapses, respectively.

In all cases, different implantation scenarios were tested and the corresponding valve functionality was examined. All chordae were placed at the insertion areas recommended for each device, i.e. free margin for NC and belly insertion for H-MRS. Then, modified trajectories were tested for each scenario, i.e. from a posterior access site (vertically aligned) corresponding to a reference angle $\alpha=0°$, to three more anterior access sites, marked by reference angles equal to $\alpha=20°$, 40°, and 50°, as depicted in Fig. 2.

According to the practical recommendation of the devices, the anterior access site (50°) and posterior one (0°) are technically not feasible for NC and H-MRS, respectively. Nevertheless, in order to obtain a complete comparison between different techniques, we extended the angle

of the access to the minimum/maximum range reported in the clinical procedures for both devices (see Fig. 3) [32], [33], [34], [35], [36], [37].

Leaflets were modelled with 10′423, 9′721 and 9′507 for Barlow, Forme Frusta and FED, respectively. In all cases the mesh is made by 2D triangular elements, adopting the isotropic hyperelastic incompressible constitutive law based on a 5th order reduced polynomial strain energy potential formulation. Chords were modelled as linear elastic trusses, with Young modulus (E) equal to 40 MPa, [38, 39]; In the neochord procedure, artificial chords are usually obtained from e-PTFE CV-4 Gore-Tex sutures, tied to the leaflet margin with a girth hitch knot approach, resulting in two suture stands pulled in the same direction [40]. In the model, each artificial chord was represented by linear truss elements with a circular cross-section of 0.148 mm2. The neochord's Young modulus was determined experimentally by performing tension testing on an e-PTFE wire. For the test, the wire was settled on the tensile testing machine (Zwick-Roll, Zwick GmbH & Co.KG, Zwick USA) in a wet environment of saline solution at a temperature of 37°, to recreate physiological conditions. Results suggested a value of the Young modulus equal to 2.3 GPa for the CV-4 Gore-Tex suture.

2.2. Finite element simulations

MV dynamics was simulated by means of the FEA provided by the commercial software for structural analysis ABAQUS (SIMULIA, Providence, RI).

Leaflets and chords were represented by linear triangular membrane elements (2D elements) and truss (1D elements), respectively.

The physiological intra-leaflets insertion of the native chords, which consists in the natural continuity of native chordae and the leaflet [41], was mimicked by imposing the same spatial node pattern in the discretization for the free margin and by merging the overlapped nodes, as described in our previous work [27]. The NC implant was simulated by applying the connection close to the free margin (4 mm from the free margin) of the diseased portion; whereas for the H-MRS implant the connection was made around the belly (7–8 mm into the leaflet body) of the same prolapse segment, see Fig. 2.

The stitching points of the leaflet, for each prolapse type and device, were equally spaced on the prolapse width (12 mm for FED and FF, 14 mm for Barlow). Ventricle access positions were defined starting from our reference position (0° - posterior access) aligned with the papillary muscles with the support of CT-scan images representative of the entire ventricle volume.

In all in-silico repairs, the closed configuration (systolic phase) was achieved by applying spatially uniform pressure to the ventricular side of the MV leaflets. In the early phase ($t/T<0.2$,

where T is the duration of the simulation), the pressure load increased linearly from zero to 120 mmHg, corresponding to the maximum pressure exerted by the ventricle contraction in systole and, consequently, to the worst condition for MV sealing. From $t/T \geq 0.2$, a steady pressure condition was applied, to model the valve repairing. In all the cases, the annulus was maintained fixed during the closure. Preliminary simulations comprising the MV annulus motion were performed for the Barlow case. The MV annulus movement results rather uninfluential on the coaptation between anterior and posterior leaflets at the end of the simulation. Moreover, the closing characteristics of the valve after the complete tensioning/repair ($t/T = 1$) does not change when imposing the annuls dynamic (see Supplemental Information for more details). However to obtain a more realistic simulation of the native chordae tensioning and the valve closure, the PMs displacements obtained from the patient-specific imaging were applied [42].

The artificial chords were tensioned all together, by applying the same displacement to each chord to achieve the maximum leaflet's coaptation. In detail, the tensioning was performed by prescribing at the free side nodes of the artificial sutures the same outward displacement along the longitudinal direction of the suture according to the initial trajectory. During the virtual repair, the sutures were not tensioned until the pressure load was maximum, i.e., the valve achieved the initial prolapse condition. In this stage of the simulation, the distal end of the chord is attached to the leaflet, whereas the proximal portion is free to move, similarly to what is observed outside the ventricle in the operating room before the tensioning/fixing stage. The artificial chords were then tensioned together. Tensioning was performed by imposing the same outward displacement at the free end of all the artificial sutures in the longitudinal direction. Details of the tensioning procedure adopted are presented in [40].
It is worth noting that the displacement that ensured the maximum coaptation area was different for each scenario, as it is directly related to the access site and the position of the suture at the leaflet-end. In order to define this displacement (d) the position of the chords was modified during the simulation linearly from 0 to 10 mm. Within this range of displacements, we were able to identify the tensioning configuration that maximizes the contact area (CA) between anterior and posterior leaflets, for each patient and entry site.
Accordingly, the optimal values of F and d, able to solve the prolapse, were identified as those producing the maximum CA for each specific case. Moreover, the maximum LS resulting in this condition was also evaluated for each case.

3. Results

The values of the displacement (*d)*, Contact Area (*CA)*, Tensioning Forces (*F)*, and Leaflet's Stress (*LS)* for each prolapse type are summarized in Fig. 3 and Table 2. Results computed for both the *NC* and *H-MRS* procedure are showed as a function of the angle access site *α*.

3.1. Barlow prolapse case (B)

In *NC* procedure model we observed a progressive increase of *d* (passing from 2.0 to 10.0 mm) with the progressive widening of *α* from 0° to 50° Differently, in the *H-MRS* device models we found that the minimum *d* (4.0 mm) was observed for *α* = 20°, while, for higher values of *α*, to obtain a competent *MV* the required *d* is nearly 8 mm (Fig. 3, panel a). With those *d* values, *CA* is mostly constant for both procedure, as shown in panel b. Specifically, we reached a *CA* of 5.5–5.7 cm^2 for *NC* and 4.8–5.0 cm^2 for *H-MRS*.

Panels c-d show the force *F* and the maximum *LS*. Both these parameters are influenced by the angle *α*. For *NC* a small increase of F and LS is recorded as a function of α. For *H-MRS* slightly higher values with *F* (about 4.1 N) and *LS* (about 0.75 MPa) are recorded for the same angles. The worst stress condition LS of 1.1 and 0.9 MPa is reached at α = 40° and 50°, for *NC* and *H-MRS*, respectively.

3.2. Forme fruste prolapse case (FF)

In the *NC* approach *d* increases as *α* increases, passing from 1 to 9.5 mm when *α* grows from 0° to 50° Viceversa, the *H-MRS* procedure seems less affected by *α*, reaching the optimum *MV* for *d* in a restrained range of 5.6–7.5 mm (see Fig. 3, panel e). In both cases, *CA* slightly increases with *α*, presenting a mean value of 4.2 and 3.8 cm^2 for *NC* and *H-MRS*, respectively (panel f).

As observed for *d*, in the *NC* procedure both *F* and *LS* increase with *α*, as shown in panels g and h, where *F* and *LS* pass from 2.9 N and 0.4 MPa for *α* = 0° to 5.7 N and 1.1 MPa for α = 50° Except for α = 40°, where *F* = 5.3 N and *LS* = 1.0 MPa, small variations of these parameters are observed for the *H-MRS* procedure, with *F* and *LS* ranging between 3.4 to 4.2 N and 0.7 to 0.8 MPa, respectively.

3.3. Fibroelastic deficiency prolapse case (FED)

When α is <50°, *d* is significantly lower for *NC* procedure than for *H-MRS* (estimated *d* between 4.3 and 6.8 mm and between 9.3 and 9.9 mm for *NC* and *H-MRS* respectively). When α = 50°, *d* values are about 7.5 mm for both techniques (Fig. 3, panel i). Further, higher values of *CA* are computed for *NC* when compared to *H-MRS* (average values of 4.2 cm^2 VS 3.7 cm^2). This difference becomes greater when *α* = 50°,

with a corresponding *CA* of 3.4 cm^2 for the *H-MRS* case (panel j), and a stable CA value for *NC*.

For NC, *F* falls within the range 2.2 - 2.7 N. For *H-MRS* approach, an opposite trend is observed, *F* decreasing from 9.9 N to 3.0 N, corresponding to α = 50 (Panel k). *LS* remains almost unchanged with *α* for the *NC* approach, as shown in panel l, while for *H-MRS* model it decreases similarly to *F* with maximum values observed for the posterior access site, i.e., 4.1 MPa for α = 0° (decreasing to 2.1 at α = 50°).

3.4. Chords-leaflets interactions

Our simulation also investigates the potential interaction among the artificial chorde and the other structures composing the *MV* apparatus, by quantifying the contact pressure on the leaflet due to the impact with the artificial chorde. Results for the *B*'s case are displayed in Fig. 4. The valve is shown in a fictitious open position to appreciate the pressure distribution at the inner surface of the *closed anterior leflet (AL)*. The color map reports the values computed at the systolic peak, when the maximum *CA* is reached. Results for both devices indicate that no interference between artificial sutures and *AL* occurs in the closing phase, when the access site is *α* = 0° Accordingly, the contact pressure is similar to the physiological one observed between the *MV* native structures (0.05 MPa). When *α* increases the contact pressure close to the leaflet free margin also increases, reaching 0.15 MPa for *α* = 50° Similar stress distributions and values were found for *FF* and *FED* models (not shown).

4. Discussion

The present study demonstrates that the use of different devices and different left ventricle (LV) access sites to treat different degenerative MV subsets can potentially modify the forces applied on the implanted chords, the leaflet coaptation length after repair, and their interaction with the anterior leaflet.

According to the Transapical Artificial Chordae Tendinae (TACT) trial results [43], a more posterior LV access site for the deployment of multiple chorde was preferable to a more anterior access, because it allowed a good chorde-papillary muscle alignment and therefore a more physiological trajectory. Present results confirmed this recommendation, showing that for NC procedure, an access site of α=0° minimizes both the *F* and the *LS* in all MV pathologies [44].

The evaluation of the entire spectrum of degenerative MV disease [28] enabled us to assess the impact of the different anatomical MV features on procedural results. *MV* prolapse can range from a simple chordal rupture involving an isolated segment (*FED*) to a multi-segment prolapse with redundant and thickened leaflet tissue (*B*). In this context, the comparison between NC and H-MRS procedures through in-silico simulations, helps to evaluate quantitatively the effects of the leaflet attachment point and ventricular insertion site on the restoration of the MV function [10, 44].

When treating FF prolapses with NC procedure, a more anterior LV access site provides larger final *d* values, but, on the other side, it has only a small effect of CA, and it is related to F and LS values that can be twice compared to those observed for the posterior LV access site in the FF model. Hence, with posterior access sites the risk of leaflet tissue tearing is sensibly lower.

Differently, *H-MRS* system seems to be less affected by the angle α for *B* and *FF* prolapse. However, it is worth noting that in all simulations of *H-MRS* procedure here presented, the performance in terms of *CA* was always lower than the one obtained for *NC* procedure, probably as a consequence of the different chorde anchoring area. For this reason, when a more anterior access site has to be selected, a careful evaluation of the device type should be carried out, based on the expected tissue overlap and the total forces (F and LS) needed to achieve that value.

The above results suggests that the access site has to be carefully selected on the base of the device chosen. As shown by the *in-silico* analyses, the advantage of the *NC* approach derives from the capability of recreating a more physiological leaflet shape at the systolic peak, making the whole length of the leaflet collaborative and overlapping the anterior leaflet.

The numerical analyses also indicate that the use of the *H-MRS* is hindered by *MV* anatomy. In particular, when treating FED disease, *NC* procedure should be preferred to H-MRS since

all the analysed parameter are in favor of NC. The worse results of H-MRS in the FED subset are probably related to the smaller leaflet lenght and therefore smaller area available for chordal deployment that usually characterize FED anathomy.

Furthermore, for the anterior working angles, the coupling of the artificial sutures with the other structures of the *MV* might significantly alter the final leaflets configuration and therefore the optimal restoration of the closure. The evidence of possible disadvantageous interference with *AL* is evident if the valve function is restored through an excessive anterior access site. The results obtained from a series of simulations, specifically designed and focused on computing the contact among sutures and *AL* (see Fig. 4), show that the anterior access site generates an un-physiological impact due to the cyclical opening of the *MV,* as consequence, it may result into tearing of the anterior leaflet.

It is to underline that the present study is based on the analysis of three models, preventing us to provide any general consideration. As future developments, we are planning to extend the presented numerical model to a larger sample, by applying a population-specific approach. Such analyses aim to generalize our results for all anatomical subsets, to help physicians in defining the standard of MV prolapse treatment using the beating-heart transapical approach. Finally, we can speculate that differences between the three patient-specific geometries, as leaflets lengths, prolapse width and valve area, are the most influencing parameters in determining the leaflet overlap. Consequently, they determine the final restoration of MV function in terms of F and LS.

5. Limitation of the study

Some literature works suggested that mitral leaflets' tissue composition may differ among the three valve prolapse types here considered [28, 29], i.e. B, FED and FF prolapse may present different mechanical response. However, current knowledge about tissue composition in degenerative mitral valve disease seems far from being sufficiently detailed to allow the adoption of mechanical models differentiated between B, FED and FF. We hence decided to mimick the mechanical response according to a unique model formulation, irrespective of the prolapse type

The clinical optimization of the *anterior leaflet* prolapse is not directly investigated in the present study and it still represents an open issue deserving specific analysis. Indeed, our methodology applied to the anterior prolapse may give indications differing from the *MV* posterior prolapse, due to the different anatomy and structural position of the leaflet. Therefore, we expect that the access site and stitching position, in the case of anterior prolapse repair, could have a significant effect on the results thus differently influencing the procedural planning.

This patient-specific study suggests that the use of in silico analysis for different valve anatomies can provide important information from the clinical point of view and support the pre-operative planning of the implants. The extension of the methodology to a larger data sample, leading to the possibility to define a population-specific model of MV prolapse, could further improve the results, because it can take in to account all the main features of interest for a certain population with the aim of an optimization of the artificial implant.
No validation was performed by comparing clinical outcomes and simulation results. However, our clinical experience with the neochord procedure confirms that the posterior implantation of artificial chords in a patient with severe MR and anatomical type A and B, [45], presents good clinical follow-up (up to 3 years) in terms of reduction of MV prolapse, valve sealing and hemodynamic recovery [35, 46]. In addition, an excessively anterior ventricular access site, on the basis of previous clinical experience [47], as well as computed tomography analysis and biosimulator tests, confirm a significant risk of interference with anterior leaflet and chord that may lead to leaflet rupture.

6. Conclusion

Our findings demonstrate that our methodological approach can be used to investigate the effects of different transapical beating-heart chordal implantation systems and of different technical aspects on all the subsets of degenerative MV disease.
The differences found in LS distribution and F suggest that the selection of the implant device should be based on the entry site and the prolapse type.

The analysis suggests that: *i)* the *NC* seems to be a preferable solutions to reach *CA* and maintaining operative *LS*, if used with a posterior entry site; *ii)* the *H-MRS*, albeit with greater values in terms of *F* and *LS*, can experience better results if used with an anterior access entry site; *iii)* for *FED* prolapse the leaflet sticking point is determinant in the effective restoration of the valve, likely due to the small amount of tissue present in this type of prolapse; and *iv)* there is evidence of contacts between artificial sutures and *AL* when the strings are implanted anteriorly. It is however recognized that to extend these results to the population of the three types of MV diseases a larger amount of cases needs to be investigated.

Acknowledgments

Authors thank Fondazione Cariparo, Padova, Italy, for funding Ph.D. fellowship of Luigi Di Micco. The Fondazione Cariparo had no involvement in the study design, in the collection, analysis, and interpretation of data, in the writing of the manuscript, and in the decision to submit the manuscript for publication.

References

1] Demetrio P, Andrea C, Gianclaudio F, Antonio M, Gino G, Carlo O. Transesophageal echocardiography in NeoChord procedure. Ann Card Anaesth 2015;18(2):191–7. https://doi.org/10.4103/0971-9784.154473.

[2] Colli A, et al. Acute safety and efficacy of the NeoChord procedure. Interact Cardiovasc Thorac Surg 2015;20(5):575–81. https://doi.org/10.1093/icvts/ivv014.

[3] Colli A, et al. TEE-guided transapical beating-heart neochord implantation in mitral regurgitation. JACC: Cardiovascular Imaging 2014;7(3):322–3. https://doi.org/10.1016/j.jcmg.2014.01.003.

[4] Colli A, et al. Transapical off-pump mitral valve repair with Neochord implantation: early clinical results. Int J Cardio. 2016;204:23–8. https://doi.org/10.1016/j.ijcard.2015.11.131.

[5] Gerosa G, D'Onofrio A, Besola L, Colli A. Transoesophageal echo-guided mitral valve repair using the Harpoon system. Eur J Cardiothorac Surg 2018;53(4):871–3. https://doi.org/10.1093/ejcts/ezx365.

[6] Colli A, et al. Transapical off-pump mitral valve repair with Neochord Implantation (TOP-MINI): step-by-step guide. Ann Cardiothorac Surg 2015;4(3):295.

[7] Colli A, et al. Transapical NeoChord mitral valve repair. Ann Cardiothorac Surg 2018;7(6):812.

[8] Colli A, Bizzotto E, Pittarello D, Gerosa G. Beating heart mitral valve repair with neochordae implantation: real-time monitoring of haemodynamic recovery. Eur J Cardiothorac Surg 2017;52(5):991–2. https://doi.org/10.1093/ejcts/ezx250.

[9] Colli A, et al. One-year outcomes after transapical echocardiography-guided mitral valve repair. Circulation 2018;138(8):843–5.

[10] Colli A, et al. Patient-specific ventricular access site selection for the NeoChord mitral valve repair procedure. Ann Thorac Surg 2017;104(2):e199–202. https://doi.org/10.1016/j.athoracsur.2017.03.082.

[11] Gammie JS, et al. Transapical beating-heart mitral valve repair with an expanded polytetrafluoroethylene cordal implantation device. Circulation 2016;134(3):189–97. https://doi.org/10.1161/CIRCULATIONAHA.116.022010.

[12] Gerosa G, D'Onofrio A, Besola L, Colli A. Transoesophageal echo-guided mitral

valve repair using the Harpoon system. Eur J Cardiothorac Surg 2017;00(January): 1–3. https://doi.org/10.1093/ejcts/ezx365.
[13] Kong F, et al. Finite element analysis of annuloplasty and papillary muscle relocation on a patient-specific mitral regurgitation model. PLoS ONE 2018;13(6): e0198331. https://doi.org/10.1371/journal.pone.0198331.
[14] Rim Y, Laing ST, McPherson DD, Kim H. Mitral valve repair using ePTFE sutures for ruptured mitral chordae tendineae : a computational simulation study. Ann Biomed Eng 2014;42(1):139–48. https://doi.org/10.1007/s10439-013-0908-1.
[15] Biglino G, Capelli C, Bruse J, Bosi GM, Taylor AM, Schievano S. Computational modelling for congenital heart disease: how far are we from clinical translation? Heart 2017;103(2):98–103. https://doi.org/10.1136/heartjnl-2016-310423.
[16] Sturla F, et al. Biomechanical drawbacks of different techniques of mitral neochordal implantation: when an apparently optimal repair can fail. J Thorac Cardiovasc Surg 2015;150(5):1303–12. https://doi.org/10.1016/j. jtcvs.2015.07.014.
[17] S. Wei, M. Caitlin, and P. Thuy, “Computational modeling of cardiac valve function and intervention,” vol. 118, no. 24, pp. 6072–6078, 2014, doi: 10.1002/ cncr.27633.Percutaneous.
[18] Kunzelman K, Reimink MS, Verrier ED, Cochran RP, Frater RWM. Replacement of mitral valve posterior chordae tendineae with expanded polytetrafluoroethylene suture: a finite element study. J Card Surg 1996;11(2):136–45. https://doi.org/ 10.1111/j.1540-8191.1996.tb00029.x.
[19] Reimink MS, Kunzelman KS, Verrier ED, Cochran RP. The effect of anterior chordal replacement on mitral valve function and stresses: a finite element study. ASAIO J 1995;41(3):M754–62.
[20] Gaidulis G, Votta E, Selmi M, Aidietien S. Numerical simulation of transapical off-pump mitral valve repair with neochordae implantation. Technol Health Care 2018;26. https://doi.org/10.3233/THC-182510.
[21] Avanzini A. A computational procedure for prediction of structural effects of edge-to-edge repair on mitral valve. J Biomech Eng 2008;130(3):031015. https://doi. org/10.1115/1.2913235.
[22] Avanzini A, Donzella G, Libretti L. Functional and structural effects of

percutaneous edge-to-edge double-orifice repair under cardiac cycle in comparison with suture repair. Proc Inst Mech Eng Part H J Eng Med 2011;225(10):959–71. https://doi.org/10.1177/0954411911414803.
[23] Sturla F, Redaelli A, Puppini G, Onorati F, Faggian G, Votta E. Functional and biomechanical effects of the edge-to-edge repair in the setting of mitral regurgitation: consolidated knowledge and novel tools to gain insight into its percutaneous implementation. Cardiovasc Eng Technol 2015;6(2):117–40. https://doi.org/10.1007/s13239-014-0208-4.
[24] Colli A, Besola L, Bizzotto E, Peruzzo P. Adult : mitral valve : cardiothoracic imaging edge-to-edge mitral valve repair with transapical neochord implantation. J. Thorac. Cardiovasc. Surg. 2018;156(1):144–8. https://doi.org/10.1016/j.jtcvs.2018.02.008.
[25] Choi A, Mcpherson DD, Kim H. Computational virtual evaluation of the effect of annuloplasty ring shape. Int J Numer Method Biomed Eng 2016;02831 (September):1–11. https://doi.org/10.1002/cnm.2831.
[26] Rim Y, McPherson DD, Chandran KB, Kim H. The effect of patient-specific annular motion on dynamic simulation of mitral valve function. J Biomech 2013;46(6): 1104–12. https://doi.org/10.1016/j.jbiomech.2013.01.014.
[27] Di Micco L, et al. The neochord mitral valve repair procedure: numerical simulation of different neochords tensioning protocols. Med Eng Phys 2019. https://doi.org/10.1016/j.medengphy.2019.09.014.
[28] Adams DH, Rosenhek R, Falk V. Degenerative mitral valve regurgitation: best practice revolution. Eur. Heart J. 2010;31(16):1958–67. https://doi.org/10.1093/eurheartj/ehq222.
[29] Hjortnaes J, et al. Comparative histopathological analysis of mitral valves in barlow disease and fibroelastic deficiency. Semin Thorac Cardiovasc Surg 2016;28 (4):757–67. https://doi.org/10.1053/j.semtcvs.2016.08.015.
[30] Atehortua A, Zuluaga MA, Garcia JD, Romero E. Automatic segmentation of right ventricle in cardiac cine MR images using a saliency analysis. Med Phys 2016;43 (12):6270–81. https://doi.org/10.1118/1.4966133.
[31] Rim Y, Choi A, McPherson DD, Kim H. Personalized computational modeling of mitral valve prolapse: virtual leaflet resection. PLoS ONE 2015;10(6):1–15.

https://doi.org/10.1371/journal.pone.0130906.
[32] Colli A, et al. Acute intraoperative echocardiographic changes after transapical off-pump mitral valve repair with NeoChord implantation. Int J Cardiol 2018;257 (November 2015):230–4. https://doi.org/10.1016/j.ijcard.2018.01.026.
[33] Colli A, et al. Patient-specific ventricular access site selection for the NeoChord mitral valve repair procedure. Ann Thorac Surg 2017;104(2):e199–202. https://doi.org/10.1016/j.athoracsur.2017.03.082.
[34] Colli A, et al. Prognostic impact of leaflet-to-annulus index in patients treated with transapical off-pump echo-guided mitral valve repair with NeoChord implantation. Int J Cardiol 2018;257(November 2015):235–7. https://doi.org/10.1016/j.ijcard.2018.01.049.
[35] Colli A, et al. Learning curve analysis of transapical NeoChord mitral valve repair†. Eur J Cardiothorac Surg Aug. 2018;54(2):273–80. https://doi.org/10.1093/ejcts/ezy046.
[36] Talukder S, Duncan A, Moat N. Harpoon repair for mitral regurgitation : a case report. Cardiovascular Imaging Case Reports 2018;3(1):22–4. https://doi.org/10.1016/j.case.2018.04.010.
L. Di Micco et al.
Medical Engineering and Physics 101 (2022) 103773
9[37] Gerosa G, D'Onofrio A, Besola L, Colli A. Transoesophageal echo-guided mitral valve repair using the Harpoon system. Eur J Cardiothorac Surg 2018;53(4):871–3. https://doi.org/10.1093/ejcts/ezx365.
[38] Kunzelman K, Reimink MS, Verrier ED, Cochran RP, Frater RWM. Replacement of mitral valve posterior chordae tendineae with expanded polytetrafluoroethylene suture: a finite element study. J Card Surg 1996;11(2):136–45. https://doi.org/10.1111/j.1540-8191.1996.tb00029.x.
[39] Lau KD, Diaz V, Scambler P, Burriesci G. Medical engineering & physics mitral valve dynamics in structural and fluid – structure interaction models. Med Eng Phys 2010;32(9):1057–64. https://doi.org/10.1016/j.medengphy.2010.07.008.
[40] di Micco L, et al. The neochord mitral valve repair procedure: numerical simulation of different neochords tensioning protocols. Med Eng Phys 2019. https://doi.org/10.1016/j.medengphy.2019.09.014.

[41] Muresian H. The clinical anatomy of the mitral valve. Clin Anat 2009;22(1):85–98. https://doi.org/10.1002/ca.20692.
[42] Votta E, Caiani E, Veronesi F, Soncini M, Montevecchi FM, Redaelli A. Mitral valve finite-element modelling from ultrasound data: a pilot study for a new approach to understand mitral function and clinical scenarios. Philos Trans R Soc, A 2008;366 (1879):3411–34. https://doi.org/10.1098/rsta.2008.0095.
[43] Seeburger J, et al. Off-pump transapical implantation of artificial neo-chordae to correct mitral regurgitation: the tact trial (transapical artificial chordae tendinae) proof of concept. J Am Coll Cardiol 2014;63(9):914–9. https://doi.org/10.1016/j. jacc.2013.07.090.
[44] Colli A, et al. CT for the transapical off-pump mitral valve repair with neochord implantation procedure. JACC: Cardiovascular Imaging 2017;10(11):1397–400. https://doi.org/10.1016/j.jcmg.2017.03.011.
[45] Colli A, et al. One-year outcomes after transapical echocardiography-guided mitral valve repair. Circulation, 138. Lippincott Williams and Wilkins; 2018. p. 843–5. https://doi.org/10.1161/CIRCULATIONAHA.118.033509.
[46] Colli A, Bizzotto E, Pittarello D, Gerosa G. Beating heart mitral valve repair with neochordae implantation: real-time monitoring of haemodynamic recovery. Eur J Cardiothorac Surg Nov. 2017;52(5):991–2. https://doi.org/10.1093/ejcts/ezx250.
[47] Seeburger J, et al. Off-pump transapical implantation of artificial neo-chordae to correct mitral regurgitation: the tact trial (transapical artificial chordae tendinae) proof of concept. J Am Coll Cardiol Mar. 2014;63(9):914–9. https://doi.org/ 10.1016/j.jacc.2013.07.090.

Figures

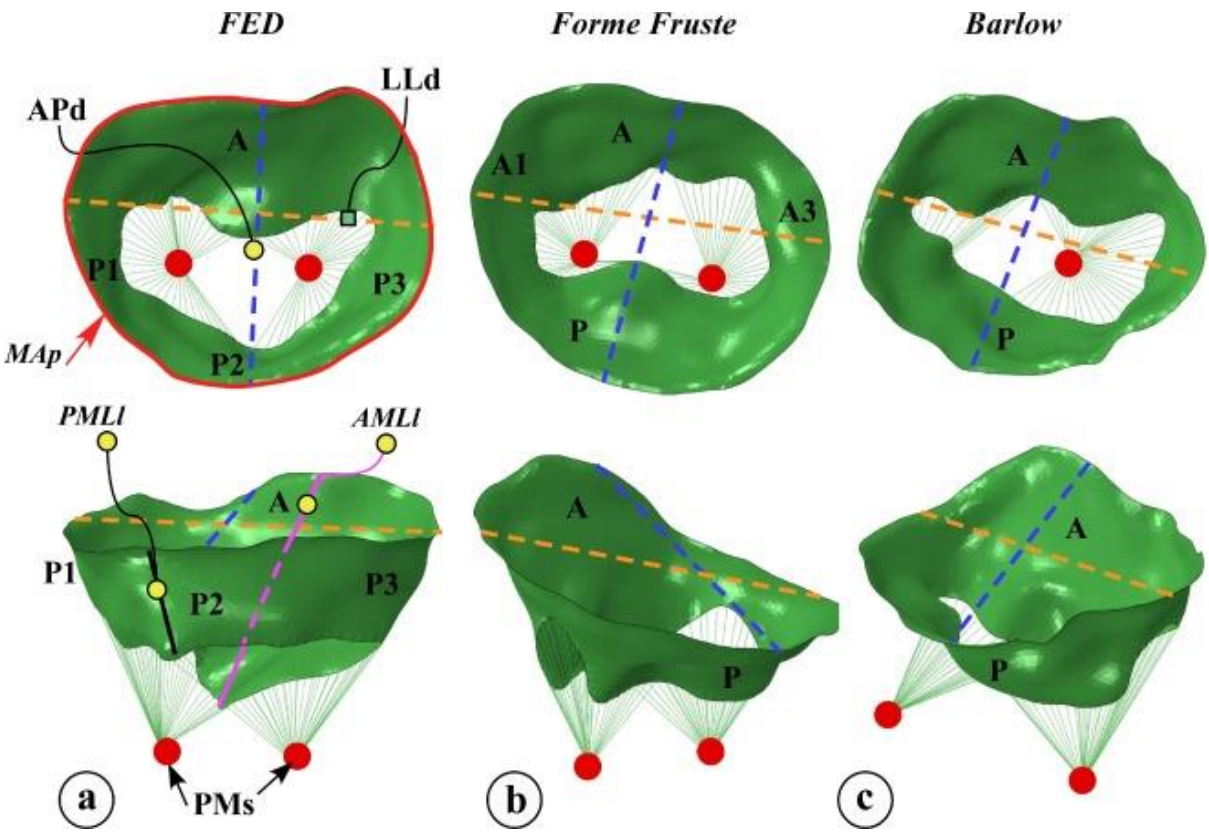

Fig. 1. MV geometry of the models at the end of diastole: From a) to c) Atrial (top-view) and lateral view (bottom) of FED, FF and, B models, respectively. A anterior leaflet, P1, P2 and P3 the posterior leaflet scallops, (APd), anteroposterior-diameter (LLd) intecommissural-distance (AMLl) anterior and (PMLl) posterior mitral leaflet lengths, the red line indicates MV annulus. CT the chordae thendinae, and PMs the papillary muscles.

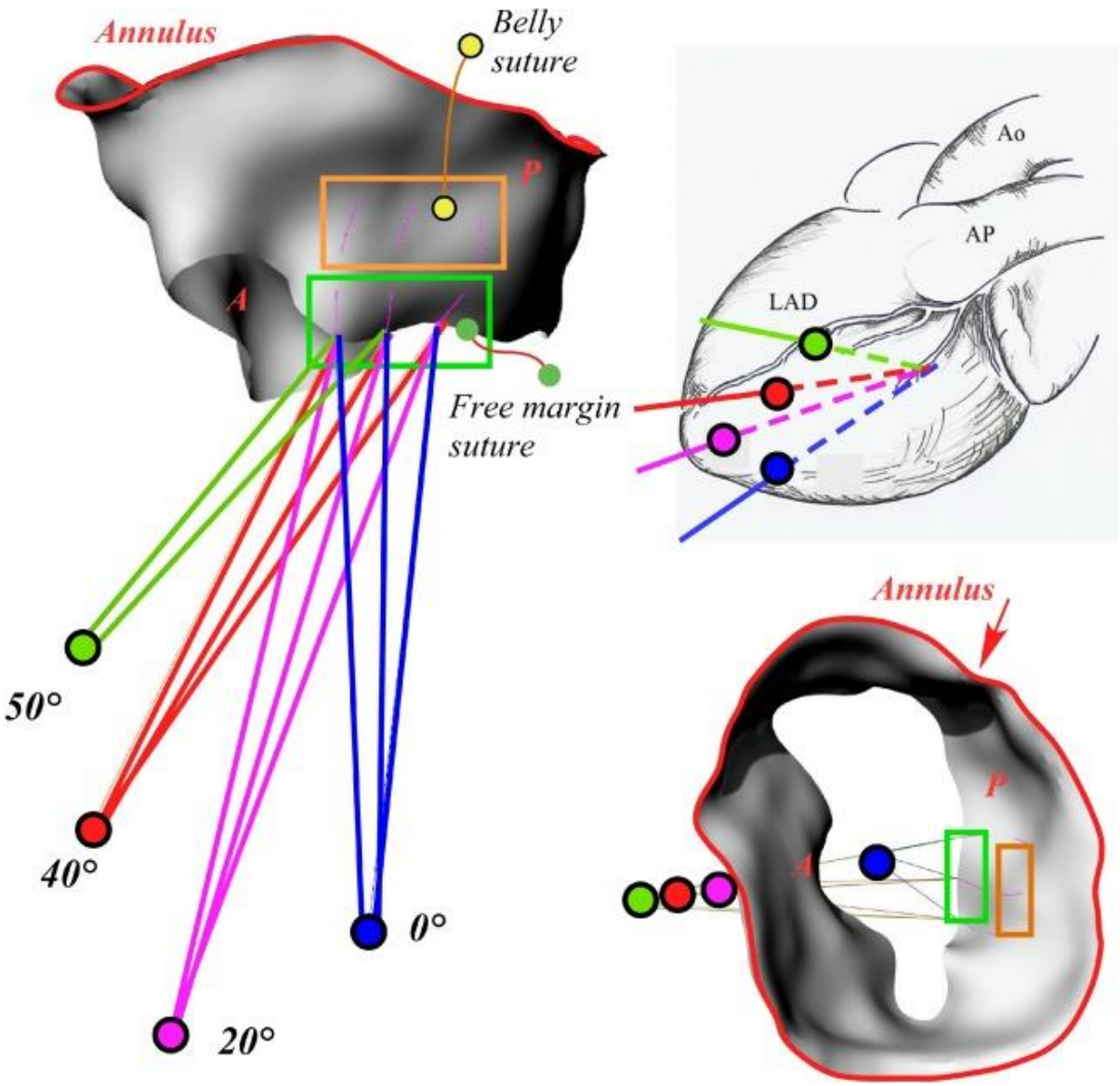

Fig. 2. Virtual repair model: The figure shows the virtual repair for B's disease. Blue lines 0°, magenta lines 20°, red lines 40°, and green lines 50°) and the different position around the diseased segment of the leaflet free margin suture (green) and the belly suture (orange).

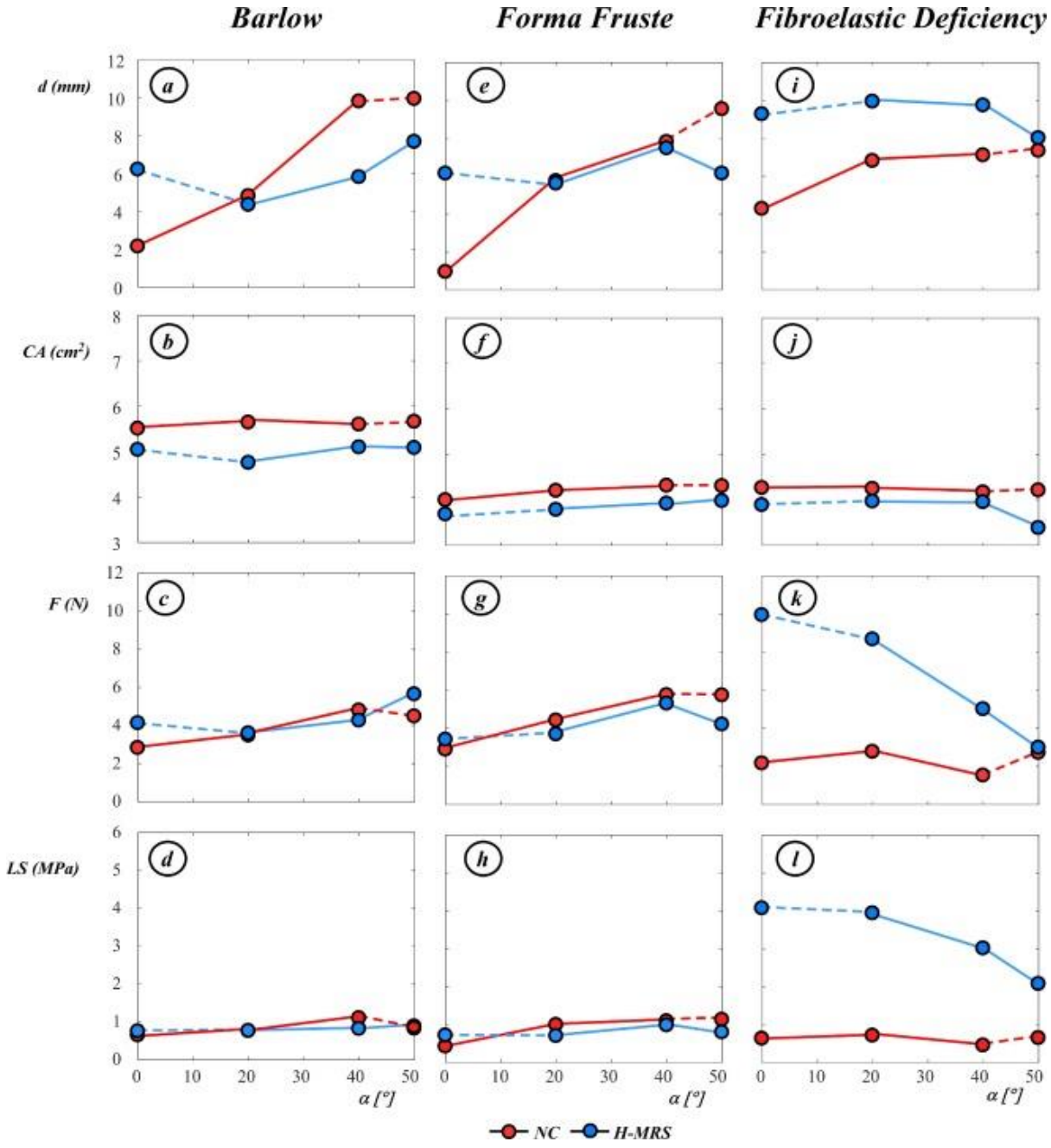

Fig. 3. Results in terms of d; CA, F, and LAS for both NC (red points) and H-MRS (blue points) leaflet grasp and for different entry site (angle (°) – 0, 20, 40, and 50) for all types of prolapse (FED, FF and B); Dotted lines indicate the extended angle of the access (α) out of the thresholds range values reported in the clinical procedures for both devices.

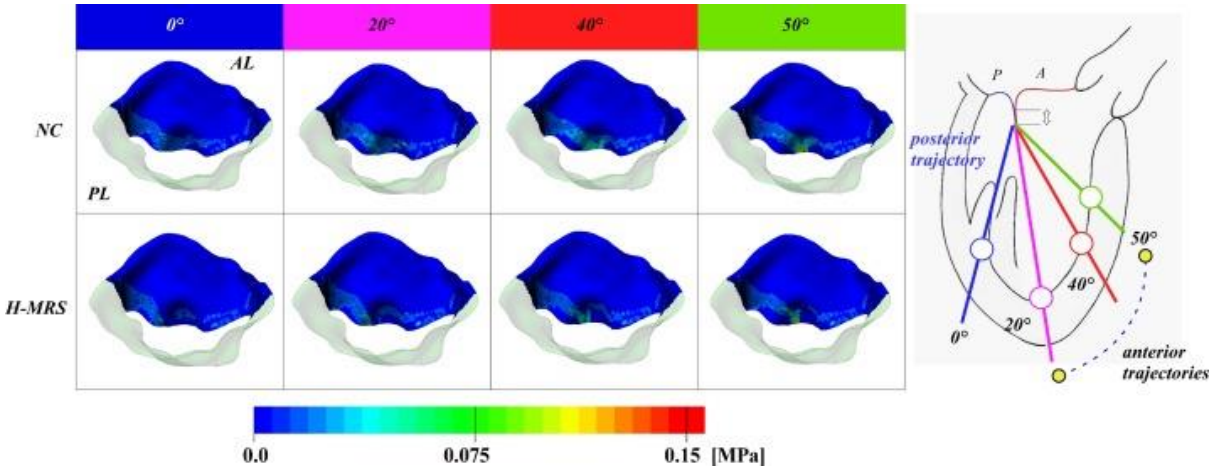

Fig. 4. Contact pressure between artificial sutures and AL for both devices (top: NC; bottom: H-MRS) for B prolapse case.

Tables

Table 1. Dimensional quantities of the MV models extract from imaging post-processing. (LLd) intecommissural-distance, (APd), anteroposterior-diameter, (AMLl) anterior and (PMLl) posterior mitral leaflet lengths, (Ls) Leaflets surface, (MAp) Annulus perimeter, end (As) Annulus surface, thickness (t), Anterior leaflet (AL), Posterior leaflet (PL).

Type	***LLd (mm)***	***APd (mm)***	***AMLl (mm)***	***PMLl (mm)***	***Ls (mm^2)***	***MAp (mm)***	***As (mm^2)***	***t (mm)***	
								AL	***PL***
B	*49.3*	*43.8*	*38.4*	*27.8*	*2333.6*	*169.9*	*1692.6*	*1.75 ± 0.43*	*1.66 ± 0.40*
FF	*46.8*	*41.1*	*35.5*	*25.2*	*2285.8*	*157.7*	*1610.1*	*1.58 ± 0.29*	*1.49 ± 0.34*
FED	*43.3*	*35.3*	*33.5*	*16.3*	*1956*	*143.8*	*1413.3*	*1.47 ± 0.32*	*1.31 ± 0.29*

Table 2. **S**ummary of the results: d (mm), CA (cm^2), F (N), LS (MPa). Results in terms of d; CA, F, and LS for both NC and H-MRS leaflet grasp and for different entry site (angle (°) – 0, 20, 40, and 50) for all types of prolapse (FED, FF and B).

		NC				***H-MRS***			
Type	***a (°)***	***d (mm)***	***CA (cm^2)***	***F (N)***	***LS (MPa)***	***d (mm)***	***CA (cm^2)***	***F (N)***	***LS (MPa)***
B	***0***	*2.1*	*5.5*	*2.8*	*0.6*	*6.2*	*5.0*	*4.1*	*0.75*
	20	*4.8*	*5.6*	*3.5*	*0.8*	*4.3*	*4.8*	*3.6*	*0.8*
	40	*9.8*	*5.6*	*4.8*	*1.1*	*5.8*	*5.1*	*4.3*	*0.8*
	50	*9.9*	*5.7*	*4.5*	*0.8*	*7.7*	*5.1*	*5.6*	*0.9*
FF	***0***	*0.9*	*4.0*	*2.9*	*0.4*	*6.1*	*3.7*	*3.4*	*0.7*
	20	*5.7*	*4.2*	*4.4*	*1.0*	*5.6*	*3.8*	*3.7*	*0.7*
	40	*7.8*	*4.3*	*5.7*	*1.1*	*7.5*	*3.9*	*5.3*	*1.0*
	50	*9.5*	*4.3*	*5.7*	*1.1*	*6.1*	*4.0*	*4.2*	*0.8*
FED	***0***	*4.3*	*4.3*	*2.2*	*0.6*	*9.3*	*3.9*	*9.9*	*4.1*
	20	*6.8*	*4.2*	*2.8*	*0.7*	*9.9*	*4.0*	*8.7*	*3.9*
	40	*6.9*	*4.2*	*1.5*	*0.4*	*9.7*	*3.9*	*5.0*	*3.0*
	50	*7.3*	*4.2*	*2.7*	*0.6*	*8.0*	*3.4*	*3.0*	*2.1*